A simplified modeling for cracked pavements

Armelle CHABOT
Laboratoire Central des Ponts et Chaussées

Quang Dat TRAN
Alain EHRLACHER
Laboratoire Analyse des Matériaux et Identification
ENPC/LCPC

INTRODUCTION

In the aim of proposing durable structures and reducing the maintenance costs incurred on French highways (a third of which undergo maintenance every year), it is highly necessary to fully comprehend the various pavement failure mechanisms that often stem from the presence of cracks. Most maintenance methods make use of several tools, whose basis constitutes an overly-simplistic mechanical model for the actual problem.

A pavement is composed by superimposing layers of different materials; its fundamental role is to distribute load in order to reduce stresses at the ground level. The French pavement design method, summarized in a published guide [LCPC-SETRA, 1994], uses results from Burmister's computation model [Burmister, 1943] of 2D axisymmetric structures. This semi-analytical model makes it possible to compute an elastic multilayer lying on a semi-infinite solid submitted to circular loading; however, incorporating the viscoelastic characteristic of asphalt layers [Duhamel *et al.*, 2003; Duhamel *et al.*, 2005], their damage [Bodin *et al.*, 2004] or the nature of cracks requires major developmental breakthroughs beyond the typical design methods [De Lurdes Antunes, 2002].

The primary objective of the work herein is to build a modeling approach better adapted to including pavement cracks. For such a model to be easily applied, a simplified theoretical and numerical framework will be introduced. This approach is intended to eventually provide a computational module in a software application for assessing and maintaining worn pavements, whose input data set contains geometry of the deteriorated pavement, regardless of the origin of cracking (material fatigue, shrinkage of hydraulic materials, ground movement, environmental effects, structural defects), its orientation (transverse, longitudinal) and density (single or multiple cracks) (see Fig. 1).

Figure 1
Example of a semi-rigid, cracked pavement

The modeling of cracked 3D pavement structures by means of finite elements is indeed possible [Batz-Villard, 1991; Vanelstrate *et al.*, 2000; Romanoschi and Li, 2002]. Yet the level of mesh refinement near cracks required to obtain significant results makes the method quite costly in terms of computation time. In order to produce a diagnostic and maintenance software that performs computations quickly and efficiently for use on worn pavements, this article will focus on developing a dedicated model.

This model, along with the method employed for solving its equations, will first be explained in summary fashion. Some validation cases will then be presented before the concluding section.

THE PROPOSED SIMPLIFIED MODEL

Notations used

(x,y,z) will denote the three coordinates of a point in reference system $(O,\mathbf{e}_1,\mathbf{e}_2,\mathbf{e}_3)$. The *n* layers of the multilayer assembly are stacked along the downward-oriented direction of the $\mathbf{e}_3$ axis of this coordinate system. Index *i* designates the layer number within the sequence {1, ..., *n*} (see Fig. 2). Layer *i* is composed of the set of points (x,y,z), such that: $z \in \left[h_i^-, h_i^+\right] \left(h_{i+1}^- = h_i^+\right)$. $e^i = h_i^+ - h_i^-$ represents layer thickness and $\overline{h}^i = \frac{h_i^+ + h_i^-}{2}$ its average dimension on the $\mathbf{e}_3$ axis. The double *i* index, i + 1 indicates the interface between layers *i* and i + 1. In the following discussion, it has been decided to denote the indices of plane tensor components by Greek letters (e.g. plane components of the stress tensor are written as $\sigma_{\alpha\beta}$).

Pavement layers *i* are chosen to be isotropic linear elastic, with Young's modulus E_i and Poisson's ratio υ_i. The soil is elastic, linear and isotropic, characterized by its Young's modulus E_s and Poisson's ratio υ_s.

Multiparticle model of multilayer materials with 5*n* equilibrium equations (designated M4-5n) for pavement layers

The multiparticle model of multilayered materials (M4) adopted for this bending problem comprises five kinematic fields for each layer *i* (i = 1, ..., n) (5n); this model makes up part of the M4 family first developed at the Ecole Nationale des Ponts et Chaussées by Chabot [1997] and Chabot and Ehrlacher [1998] to study, in elasticity, edge effects for composite structures. Let's denote $u_j(x,y,z)$

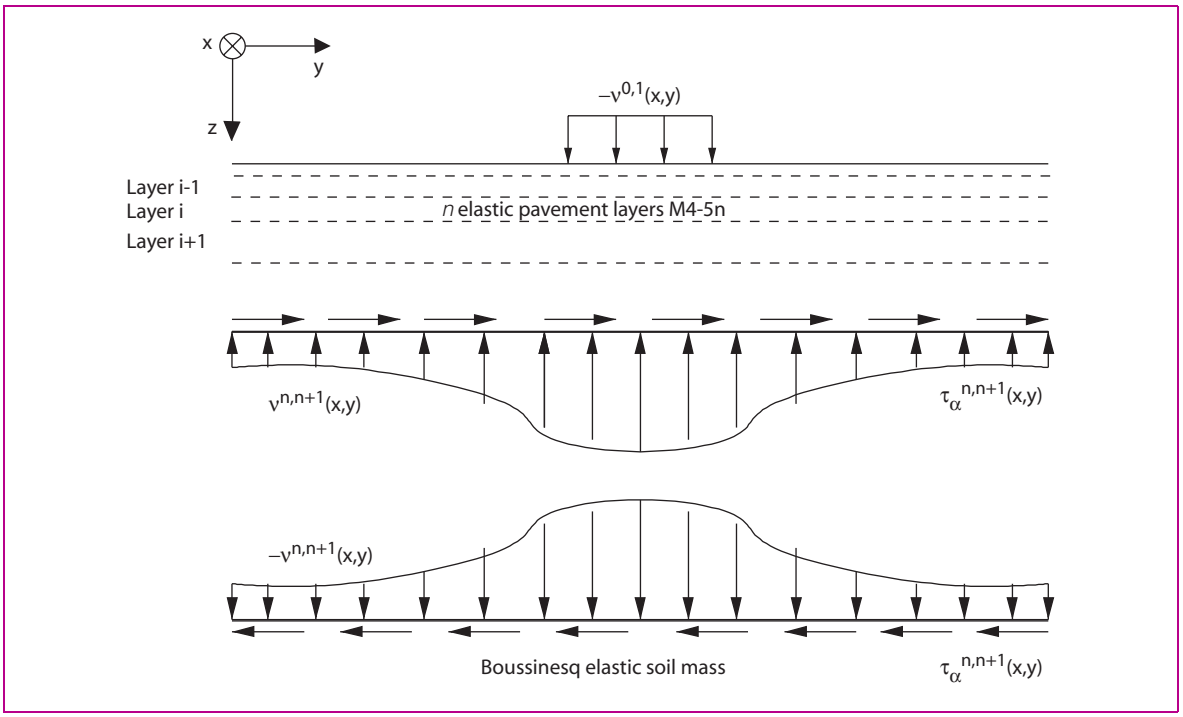

Figure 2
Diagram of the simplified M4-5nB model

(with j = 1,3) the 3D displacement fields, the kinematics of associated layers *i* (i = 1, ..., n) then contain the following average in-plane and out-of-plane displacements:

$$U_\alpha^i(x,y) = \int_{h_i^-}^{h_i^+} \frac{1}{e^i} u_\alpha(x,y,z)\,dz \text{ et } U_3^i(x,y) = \int_{h_i^-}^{h_i^+} \frac{1}{e^i} u_3(x,y,z)\,dz$$

along with the average rotations defined as follows:

$$\Phi_\alpha^i(x,y) = \int_{h_i^-}^{h_i^+} \frac{12\left(z-\overline{h}^i\right)}{e^{i3}} u_\alpha(x,y,z)\,dz$$

The M4-5n may be considered like superimposing *n* Reissner plates. Its construction relies on a 1st-degree polynomial approximation of the membrane stress fields in *z*. The expression of 3D equilibrium equations yields 2nd- and 3rd-degree polynomials in *z* per layer for shear stresses and normal stress, respectively. The coefficients of these polynomials for each layer are correlated with the classical generalized force and moment fields of Reissner plates. Such approximations offer the advantage of defining at the i, i + 1 interfaces both the shear stresses $\tau_\alpha^{i,i+1}(x,y)$ and normal stresses $v^{i,i+1}(x,y)$ such that:

$$\tau_\alpha^{i,i+1}(x,y) = \sigma_{\alpha 3}\left(x,y,h_i^+\right) = \sigma_{\alpha 3}\left(x,y,h_{i+1}^-\right) \text{ et } v^{i,i+1}(x,y) = \sigma_{33}\left(x,y,h_i^+\right) = \sigma_{33}\left(x,y,h_{i+1}^-\right)$$

The Hellinger-Reissner function [Reissner, 1950] is used herein to obtain the equations expressed in generalized variables. The actual 3D multilayered problem can then be reduced to determining fields in (x,y) for each layer *i* and each interface between layers i, i + 1, thus transforming the real 3D object into a 2D geometric object. Furthermore, the M4 model diverts focus from edge effects, resulting in a finite value of stresses at plate edges. Between two adjacent material layers, it then becomes possible to express delamination criteria in terms of interfacial forces [Chabot *et al.*, 2000; Caron *et al.*, 2004].

On finite structures, Carreira *et al.* [2002] showed, by introducing a concept of generalized finite element forces, that M4-5n fields are very close to those obtained from a refined approach involving 3D finite elements. Tran [2001] demonstrated that these fields lead to a good approximation of the stress fields present in pavement layers, of infinite in-plane dimension, lying on the soil.

In sum, after combining the various M4-5n equilibrium and constitutive equations, a system of five 2nd-order differential equations for each layer *i* of the pavement multilayer (i = 1, ..., n) in the (x,y) plane can be generated. The interested reader can refer to Tran's doctoral thesis [2004] for a complete model description. The system has been presented below under the hypothesis that volume forces and anelastic strain are both negligible:

$$e_i E_i \left(\frac{1}{1-\upsilon_i^2} U^i_{1,11} + \frac{1}{2(1+\upsilon_i)} U^i_{1,22} + \frac{1}{2(1-\upsilon_i)} U^i_{2,12} \right) = \tau_1^{i-1,i} - \tau_1^{i,i+1} \quad (1)$$

$$e_i E_i \left(\frac{1}{2(1+\upsilon_i)} U^i_{2,11} + \frac{1}{1-\upsilon_i^2} U^i_{2,22} + \frac{1}{2(1-\upsilon_i)} U^i_{1,12} \right) = \tau_2^{i-1,i} - \tau_2^{i,i+1} \quad (2)$$

$$\frac{2e_i^2 E_i}{1-\upsilon_i^2} \Phi^i_{1,11} + \frac{e_i^2 E_i}{1+\upsilon_i} \Phi^i_{1,22} + \frac{e_i^2 E_i}{1-\upsilon_i} \Phi^i_{2,12} - \frac{10 E_i}{1+\upsilon_i} \left(U^i_{3,1} + \Phi^i_1 \right) = -10 \left(\tau_1^{i-1,i} + \tau_1^{i,i+1} \right) \quad (3)$$

$$\frac{e_i^2 E_i}{1+\upsilon_i} \Phi^i_{2,11} + \frac{2e_i^2 E_i}{1-\upsilon_i^2} \Phi^i_{2,22} + \frac{e_i^2 E_i}{1-\upsilon_i} \Phi^i_{1,12} - \frac{10 E_i}{1+\upsilon_i} \left(U^i_{3,2} + \Phi^i_2 \right) = -10 \left(\tau_2^{i-1,i} + \tau_2^{i,i+1} \right) \quad (4)$$

$$U^i_{3,11} + U^i_{3,22} + \Phi^i_{1,1} + \Phi^i_{2,2} = \frac{12(1+\upsilon_i)}{5 e_i E_i} \left(v^{i-1,i} - v^{i,i+1} \right) - \frac{(1+\upsilon_i)}{5E_i} \left(\tau_{1,1}^{i,i+1} + \tau_{2,2}^{i,i+1} + \tau_{1,1}^{i-1,i} + \tau_{2,2}^{i-1,i} \right) \quad (5)$$

Similarly, a system of three 1st-order differential equations per interface i, i + 1 (i = 1, ..., n – 1) is obtained as follows:

$$U_1^{i+1} - U_1^i - \frac{5e_i}{12} \Phi_1^i - \frac{5e_{i+1}}{12} \Phi_1^{i+1} - \frac{e_i}{12} U^i_{3,1} - \frac{e_{i+1}}{12} U^{i+1}_{3,1} = -\frac{e_i (1+\upsilon_i)}{12E_i} \tau_1^{i-1,i} + \frac{1}{8} \left(\frac{2e_i (1+\upsilon_i)}{E_i} + \frac{2e_{i+1} (1+\upsilon_{i+1})}{E_{i+1}} \right) \tau_1^{i,i+1} - \frac{e_{i+1} (1+\upsilon_{i+1})}{12E_{i+1}} \tau_1^{i+1,i+2} \quad (6)$$

$$U_2^{i+1} - U_2^i - \frac{5e_i}{12} \Phi_2^i - \frac{5e_{i+1}}{12} \Phi_2^{i+1} - \frac{e_i}{12} U^i_{3,2} - \frac{e_{i+1}}{12} U^{i+1}_{3,2} = -\frac{e_i (1+\upsilon_i)}{12E_i} \tau_2^{i-1,i} + \frac{1}{8} \left(\frac{2e_i (1+\upsilon_i)}{E_i} + \frac{2e_{i+1} (1+\upsilon_{i+1})}{E_{i+1}} \right) \tau_2^{i,i+1} - \frac{e_{i+1} (1+\upsilon_{i+1})}{12E_{i+1}} \tau_2^{i+1,i+2} \quad (7)$$

$$U_3^{i+1} - U_3^i = -\frac{9e_i}{70E_i} v^{i-1,i} + \frac{13}{35} \left(\frac{e_i}{E_i} + \frac{e_{i+1}}{E_{i+1}} \right) v^{i,i+1} - \frac{9e_{i+1}}{70E_{i+1}} v^{i+1,i+2} \quad (8)$$

Forces at the n, n+1 interface between the last layer *n* at the bottom of the pavement multilayer and the ground are the unknowns to be found. They depend on the interaction (whether bonded or not) between ground and pavement structure (Fig. 2).

Boussinesq equations for the soil mass

Since the number of unknowns to be determined would have been too great, the modeling approach proceeded by cutting the semi-infinite soil mass into a M4-5n set-up of several finite-thickness layers, while providing effective solutions [Tran, 2001], still cannot serve as a basis for building a high-speed computation software. It was thus decided to utilize an analytical model for the semi-infinite elastic soil mass. The Boussinesq solution, recalled for example in [Johnson, 1992], stands out as the most viable.

The overlap of the two models proceeds by either the continuity or non-continuity of displacement fields at the n, n+1 interface of the *n* pavement layers and the ground (Fig. 2). Three additional equations yield the relation between surface displacements $u_j^{surface}(x,y)\,(j \in \{1,2,3\})$ of the

Boussinesq soil mass and M4-5n interfacial forces $\tau_\alpha^{n,n+1}(x,y)$ and $\nu^{n,n+1}(x,y)$, as presented below for the bonded case:

$$u_1^{surface}(x,y) = U_1^n(x,y) + \frac{e^n}{2}\Phi_1^n(x,y)$$

$$= \frac{(1+\upsilon_s)}{\pi E_s} \times \left(\begin{array}{l} -\frac{1-2\upsilon_s}{2}\int_S \nu^{n,n+1}(\xi,\eta)\frac{(x-\xi)}{(x-\xi)^2+(y-\eta)^2}\,d\xi d\eta \\ +\int_S \tau_1^{n,n+1}(\xi,\eta)\frac{(x-\xi)^2+(1-\upsilon_s)(y-\eta)^2}{\left((x-\xi)^2+(y-\eta)^2\right)^{3/2}}\,d\xi d\eta \\ +\upsilon_s\int_S \tau_2^{n,n+1}(\xi,\eta)\frac{(x-\xi)(y-\eta)}{\left((x-\xi)^2+(y-\eta)^2\right)^{3/2}}\,d\xi d\eta \end{array} \right) \quad (9)$$

$$u_2^{surface}(x,y) = U_2^n(x,y) + \frac{e^n}{2}\Phi_2^n(x,y)$$

$$= \frac{(1+\upsilon_s)}{\pi E_s} \times \left(\begin{array}{l} -\frac{1-2\upsilon_s}{2}\int_S \nu^{n,n+1}(\xi,\eta)\frac{(y-\eta)}{(x-\xi)^2+(y-\eta)^2}\,d\xi d\eta \\ +\upsilon_s\int_S \tau_1^{n,n+1}(\xi,\eta)\frac{(x-\xi)(y-\eta)}{\left((x-\xi)^2+(y-\eta)^2\right)^{3/2}}\,d\xi d\eta \\ +\int_S \tau_2^{n,n+1}(\xi,\eta)\frac{(1-\upsilon_s)(x-\xi)^2+(y-\eta)^2}{\left((x-\xi)^2+(y-\eta)^2\right)^{3/2}}\,d\xi d\eta \end{array} \right) \quad (10)$$

$$u_3^{surface}(x,y) = U_3^n(x,y)$$

$$= \frac{(1+\upsilon_s)}{\pi E_s} \times \left(\begin{array}{l} (1-\upsilon_s)\int_S \nu^{n,n+1}(\xi,\eta)\frac{1}{\left((x-\xi)^2+(y-\eta)^2\right)^{1/2}}\,d\xi d\eta \\ +\frac{(1-2\upsilon_s)}{2}\left(\begin{array}{l} \int_S \tau_1^{n,n+1}(\xi,\eta)\frac{(x-\xi)}{(x-\xi)^2+(y-\eta)^2}\,d\xi d\eta \\ +\int_S \tau_2^{n,n+1}(\xi,\eta)\frac{(y-\eta)}{(x-\xi)^2+(y-\eta)^2}\,d\xi d\eta \end{array} \right) \end{array} \right) \quad (11)$$

In the following discussion, we will refer to the combination of the M4-5n model for pavement layers and the Boussinesq soil model as "M4-5nB".

M4-5nB boundary conditions

Forces at the 0, 1 interface between the exterior and the first pavement layer serve as the model givens; they are correlated with the set of presumed known loading conditions of a truck wheel rolling over the pavement (Fig. 2).

In order to express the various boundary condition systems of pavement multilayer edges (or cracks) as a function of both the kinematic unknowns and interface forces, the constitutive equations of layer *i* from M4-5n are used.

On the unloaded edges (or vertical cracks) of pavement layers i (i = 1, ..., n), free edge boundary conditions are imposed. In this case, they may be expressed in the form of the five equation-per-layer

system [Tran, 2004]. For purposes of illustration, they have been listed below for any y whenever x becomes infinite (or tends to a finite value in the case of a crack):

$$\lim_{x\to\pm\infty}\left(U^i_{1,1}(x,y)+\upsilon_i U^i_{2,2}(x,y)\right)=0 \tag{12}$$

$$\lim_{x\to\pm\infty}\left(\Phi^i_{1,1}(x,y)+\upsilon_i \Phi^i_{2,2}(x,y)\right)=0 \tag{13}$$

$$\lim_{x\to\pm\infty}\left(U^i_{1,2}(x,y)+U^i_{2,1}(x,y)\right)=0 \tag{14}$$

$$\lim_{x\to\pm\infty}\left(\Phi^i_{1,2}(x,y)+\Phi^i_{2,1}(x,y)\right)=0 \tag{15}$$

$$\lim_{x\to\pm\infty}\left(\Phi^i_1(x,y)+U^i_{3,1}(x,y)+\frac{(1+\upsilon_i)}{5E_i}\left(\tau_1^{i-1,i}(x,y)+\tau_i^{i,i+1}(x,y)\right)\right)=0 \tag{16}$$

On the blocked edges of pavement layers i (i = 1, ..., n), e.g. where the material is confined and cannot move along the normal to its vertical cross-section, the boundary conditions are also expressed in the form of the five equation-per-layer system [Tran, 2004]. Again for illustration, they have been displayed below for any y whenever x becomes infinite (or tends to a finite value):

$$\lim_{x\to\pm\infty} U^i_1(x,y)=0 \tag{17}$$

$$\lim_{x\to\pm\infty} \Phi^i_1(x,y)=0 \tag{18}$$

$$\lim_{x\to\pm\infty}\left(U^i_{1,2}(x,y)+U^i_{2,1}(x,y)\right)=0 \tag{19}$$

$$\lim_{x\to\pm\infty}\left(\Phi^i_{1,2}(x,y)+\Phi^i_{2,1}(x,y)\right)=0 \tag{20}$$

$$\lim_{x\to\pm\infty}\left(\Phi^i_1(x,y)+U^i_{3,1}(x,y)+\frac{(1+\upsilon_i)}{5E_i}\left(\tau_1^{i-1,i}(x,y)+\tau_i^{i,i+1}(x,y)\right)\right)=0 \tag{21}$$

Generalization of the M4-5nB equations

To write the overall system of equations for M4-5nB, interface equations (6) to (8) are used to eliminate forces $\tau_1^{i,i+1}, \tau_2^{i,i+1}$ et $v^{i,i+1}$ (i = 1, ..., n – 1) in equations (1) through (5) (i = 1, ..., n) from M4-5n that get associated with equations (9)-(11) from Boussinesq's analytical model. Ultimately, presentation of the initial 3D problem is reduced to solving a 2D problem laid out in the plane composed of 5n+3 equations with 5n+3 plane unknown fields.

$X = {}^T\left[U^1_1, U^1_2, \Phi^1_1, \Phi^1_2, U^1_3, ..., U^i_1, U^i_2, \Phi^i_1, \Phi^i_2, U^i_3, ..., U^n_1, U^n_2, \Phi^n_1, \Phi^n_2, U^n_3\right]_{(x,y)}$ denotes the $5n$-dimensional vector of kinematic unknowns and $\Sigma = {}^T\left[\tau_1^{n,n+1}, \tau_2^{n,n+1}, v^{n,n+1}\right]_{(x,y)}$ the three-dimensional vector of static unknowns at points (x,y) in this plane.

Once the loading boundary conditions, known at the pavement multilayer surface, have been applied, system generalization can be synthesized in the form of the following global 2nd-order, $5n$-dimensional differential system:

$$AA.X_{,11} + BB.X_{,22} + CC.X_{,12} + DD.X_{,1} + EE.X_{,2} + FF.X = GG.\Sigma_{,1} + HH.\Sigma_{,2} + II.\Sigma + JJ \tag{22}$$

with: AA, BB, CC, DD, EE and FF being the corresponding material matrices, of dimension $5n \times 5n$; GG, HH and II the material matrices of dimension $5n \times 3$; and JJ the $5n$-dimensional vector that integrates loading boundary conditions at the top of the pavement multilayer and whose detailed expressions are given in Tran's doctoral thesis [2004].

This system of the three linear equations complementary to Boussinesq's equations is provided in the following form [Tran, 2004]:

$$M.X(x,y) = \int_S f(x,y,\xi,\eta)\,\Sigma(\xi,\eta)\,d\xi\,d\eta \tag{23}$$

with $M = \begin{pmatrix} 0 & 0 & 0 & 0 & 0 \ldots & 1 & 0 & e^n/2 & 0 & 0 \\ 0 & 0 & 0 & 0 & 0 \ldots & 0 & 1 & 0 & e^n/2 & 0 \\ 0 & 0 & 0 & 0 & 0 \ldots & 0 & 0 & 0 & 0 & 1 \end{pmatrix}$ being the matrix of dimension $3 \times 5n$ and f the 3×3 matrix of the expressions in (9) to (11).

Generalized for n layers, the discretized expression of the five boundary conditions for each layer i, as illustrated in equations (12) through (21) and, like before, applied at the pavement-soil interface by means of equations (6)-(8), may now be written on each plane edge in the form of the following systems of 1st-order differential equations:

For $x \to \infty$, $\forall y$

$$\begin{cases} CL_{x1}.X'_1 + CL_{x2}.X'_2 + CL_{x3}.X = CL_{x4}.\Sigma^{0,1} + CL_{x5}.\Sigma & \text{fixed boundary conditions} \\ CL_{x6}.X'_1 + CL_{x7}.X'_2 + CL_{x8}.X = CL_{x9}.\Sigma^{0,1} + CL_{x10}.\Sigma & \text{free boundary conditions} \end{cases} \quad (24)$$

For $\forall x$, $y \to \infty$,

$$\begin{cases} CL_{y1}.X'_1 + CL_{y2}.X'_2 + CL_{y3}.X = CL_{y4}.\Sigma^{0,1} + CL_{y5}.\Sigma & \text{fixed boundary conditions} \\ CL_{y6}.X'_1 + CL_{y7}.X'_2 + CL_{y8}.X = CL_{y9}.\Sigma^{0,1} + CL_{y10}.\Sigma & \text{free boundary conditions} \end{cases} \quad (25)$$

with $\Sigma^{0,1} = {}^T\left[\tau_1^{0,1}, \tau_2^{0,1}, \nu^{0,1}\right]$ being the vector of loading boundary conditions and CL_{xj}, and CL_{yj} $j \in [1,10]$ the coefficient matrices.

NUMERICAL RESOLUTION OF THE M4-5NB MODEL EQUATIONS

In order to numerically solve the set of M4-5nB model equations, the computation plane (of width l and length L) has in the present case been discretized into N intervals along the x-axis and N intervals along the y-axis (see Fig. 3). The finite differences method is chosen for this step. The unknowns are the (5n+3) values at nodes (x_k, y_l) ($k \in [1, N+1]$, $l \in [1, N+1]$) of the unknown kinematic and static fields on this surface.

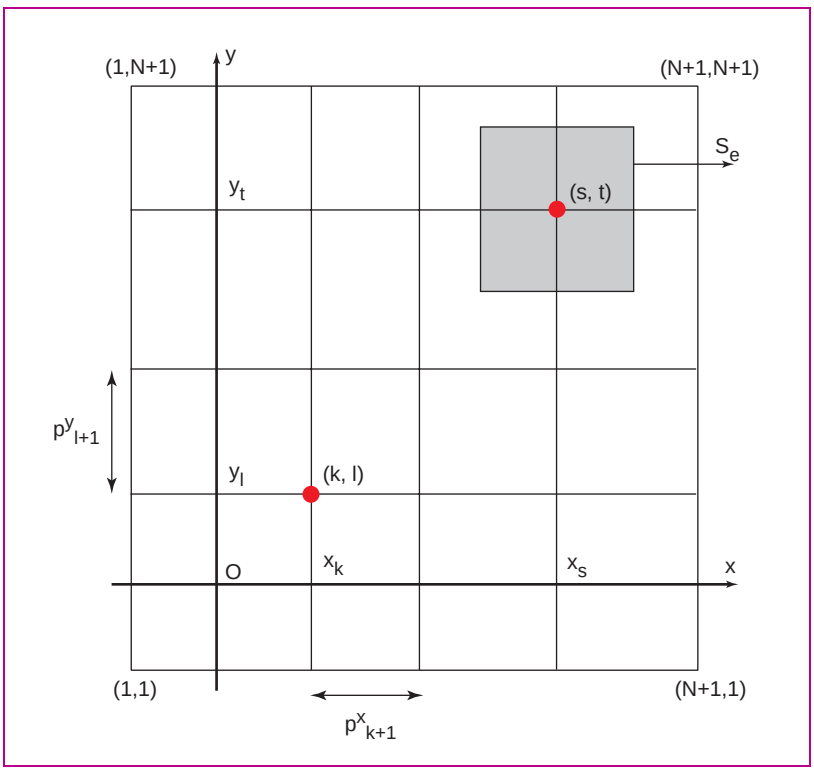

Figure 3
Discretization of the M4-5nB model computation plane

In the following discussion, $\mathbf{X}$ and __ will denote respectively the vector of kinematic unknowns with dimension $5n(N+1)^2$ and the vector of static unknowns with dimension $3(N+1)^2$ such that:

$$\mathbf{X} = {}^{T}\left[\mathbf{X}_{1,1}\,\mathbf{X}_{1,2}\ldots\mathbf{X}_{k,l}\ldots\mathbf{X}_{N+1,N+1}\right] \text{ avec } \mathbf{X}_{k,l} = \mathbf{X}(x_k, y_l)$$

$$\mathbf{\Sigma} = {}^{T}\left[\mathbf{\Sigma}_{1,1}\,\mathbf{\Sigma}_{1,2}\ldots\mathbf{\Sigma}_{k,l}\ldots\mathbf{\Sigma}_{N+1,N+1}\right] \text{ avec } \mathbf{\Sigma}_{k,l} = \mathbf{\Sigma}(x_k, y_l)$$

The overall numerical system of the problem thus has a dimension of $(5n+3)(N+1)^2$.

Numerical processing of the 5*n* pavement layer equations

To numerically solve the system in (22) with the previously-chosen discretization, the Newmark finite differences method is applied (to derive the value of $\alpha = \frac{1}{2}$) [Newmark, 1959], with the error ascribed to the method lying on the order of the discretization step to the third power, as follows for any field $\mathbf{Y}$:

$$\frac{\mathbf{Y}_{(k+1,l)'1} + \mathbf{Y}_{(k,l)'1}}{2} = \frac{\mathbf{Y}_{(k+1,l)} - \mathbf{Y}_{(k,l)}}{p^{x}_{k+1}},\ p^{x}_{k+1} = x_{k+1} - x_k \tag{26}$$

$$\frac{\mathbf{Y}_{(k,l+1)'2} + \mathbf{Y}_{(k,l)'2}}{2} = \frac{\mathbf{Y}_{(k,l+1)} - \mathbf{Y}_{(k,l)}}{p^{y}_{l+1}},\ p^{y}_{l+1} = y_{l+1} - y_l \tag{27}$$

Through use of relations (26) and (27), the system of 2nd-order differential equations in (22) gets transformed into a system of discretized linear equations.

For purposes of illustration, let's rewrite equation (22) for point couples (x_k,y_l) and (x_{k+1},y_l) in the following schematic fashion:

$$AA.\mathbf{X}_{(k,l)'11} + BB.\mathbf{X}_{(k,l)'22} + \ldots\ldots\ldots\ldots = GG.\mathbf{\Sigma}_{(k,l)'1} + HH.\mathbf{\Sigma}_{(k,l)'2} + \ldots\ldots\ldots\ldots \tag{28}$$

$$AA.\mathbf{X}_{(k+1,l)'11} + BB.\mathbf{X}_{(k+1,l)'22} + \ldots\ldots\ldots\ldots = GG.\mathbf{\Sigma}_{(k+1,l)'1} + HH.\mathbf{\Sigma}_{(k+1,l)'2} + \ldots\ldots\ldots\ldots \tag{29}$$

By taking the sum of these two equations (28) and (29) and using (26) (by first substituting $\mathbf{Y}_{,1}$ by $\mathbf{X}_{,11}$ and then $\mathbf{Y}$ by $\mathbf{\Sigma}$), the 2nd-order derivatives with respect to x are eliminated:

$$2AA\frac{\mathbf{X}_{(k+1,l)'1} - \mathbf{X}_{(k,l)'1}}{p^{x}_{k+1}} + BB(\mathbf{X}_{(k,l)'22} + \mathbf{X}_{(k+1,l)'22})\ldots = \tag{30}$$

$$2GG\frac{\mathbf{\Sigma}_{(k+1,l)} - \mathbf{\Sigma}_{(k,l)}}{p^{x}_{k+1}} + HH(\mathbf{\Sigma}_{(k,l)'2} + \mathbf{\Sigma}_{(k+1,l)'2})..$$

The same operation is once again employed to eliminate 1st-order derivatives with respect to x. For the derivatives with respect to y, the analogous method uses (27).

The resultant linear system thus contains $5n(N-1)^2$ equations, the details of which have been included in Tran's thesis [2004].

Numerical processing of the Boussinesq equations

Let's now consider the discretization of surface S into $(N+1)^2$ elementary surfaces S_e (Fig. 3). The elementary rectangular surface $S_e(x_s,y_t)$, which corresponds with the common interior point (x_s,y_t), is defined by the surface $\left[x_{s-\frac{1}{2}}, x_{s+\frac{1}{2}}\right]\times\left[y_{t-\frac{1}{2}}, y_{t+\frac{1}{2}}\right]$ $(1 < s < N+1)$ and $(1 < t < N+1)$. On the edges of surface S, the following elementary surfaces are defined:

- for $1 < t < N+1$:

$$S_e^{1,t} = \left[x_1, x_{\frac{3}{2}}\right]\times\left[y_{t-\frac{1}{2}}, y_{t+\frac{1}{2}}\right] \text{ et } S_e^{N+1,t} = \left[x_{N+\frac{1}{2}}, x_{N+1}\right]\times\left[y_{t-\frac{1}{2}}, y_{t+\frac{1}{2}}\right]$$

- for $1 < s < N+1$:

$$S_e^{s,1} = \left[x_{s-\frac{1}{2}}, x_{s+\frac{1}{2}}\right] \times \left[y_1, y_{\frac{3}{2}}\right] \text{ et } S_e^{s,N+1} = \left[x_{s-\frac{1}{2}}, x_{s+\frac{1}{2}}\right] \times \left[y_{N+\frac{1}{2}}, y_{N+1}\right]$$

- on the four corners:

$$S_e^{1,1} = \left[x_1, x_{\frac{3}{2}}\right] \times \left[y_1, y_{\frac{3}{2}}\right]; S_e^{1,N+1} = \left[x_1, x_{\frac{3}{2}}\right] \times \left[y_{N+\frac{1}{2}}, y_{N+1}\right]$$

$$S_e^{N+1,N+1} = \left[x_{N+\frac{1}{2}}, x_{N+1}\right] \times \left[y_{N+\frac{1}{2}}, y_{N+1}\right]; S_e^{N+1,1} = \left[x_{N+\frac{1}{2}}, x_{N+1}\right] \times \left[y_1, y_{\frac{3}{2}}\right]$$

To facilitate integration steps, which may be performed analytically, it has been assumed in an initial approximation that the interface forces written in vector $\boldsymbol{\Sigma}$ remain constant over these elementary surfaces S_e. The following relations are then obtained:

$$\int_S f(x,y,\xi,\eta)\boldsymbol{\Sigma}(\xi,\eta)d\xi d\eta = \sum_1^{(N+1)^2} \int_{S_e} f(x,y,\xi,\eta)\boldsymbol{\Sigma}(\xi,\eta)d\xi d\eta \qquad (31)$$

$$\approx \sum_1^{(N+1)^2} \boldsymbol{\Sigma}(\xi_s,\eta_t)\left(\int_{S_e} f(x,y,\xi,\eta)\, d\xi d\eta\right)$$

By changing variables, the integral of functions contained in $f(x,y,\xi,\eta)$ can easily be computed analytically on S_e and hence leads to the discretized form of (23) at point (x_k,y_l):

$$M.\mathbf{X}_{k,l} = \sum_1^{(N+1)^2} N_{k,l,s,t}.\boldsymbol{\Sigma}_{s,t} \quad \forall k = 1,N+1, \forall l = 1,N+1 \qquad (32)$$

Let N represent the (3×3) matrix of the expressions for integrated *f*.

The final assembly thereby yields $3(N+1)^2$ linear equations set forth as follows:

$$K_4.\mathbf{X} = K_5.\boldsymbol{\Sigma} \qquad (33)$$

with K_4 and K_5 being the matrices of dimensions $3(N+1)^2 \times 5n(N+1)^2$ and $3(N+1)^2 \times 3(N+1)^2$, respectively.

Numerical processing of the boundary conditions

To linearize boundary condition equations (24) and (25), Newmark's approximation and the relations obtained for the 5n pavement layers will, like before, both be used. With relations (26) and (30), the terms $\mathbf{X}_{(k,j)'1}$ and $\mathbf{X}_{(k+1,j)'1}$ from (24) and (25) can be written as a function of terms $\mathbf{X}_{(k,j)'2}$, $\mathbf{X}_{(k,j)'22}$, $\mathbf{X}_{(k+1,j)'2}$, $\mathbf{X}_{(k+1,j)'22}$ in a way that only introduces derivatives with respect to *y*. Once these values have been substituted into previously-discretized equations (24) and (25) and in using relation (27) twice, the derivative terms with respect to *y* can be eliminated, yielding $4 \times 5nN$ additional equations on the four edges of the discretized plane (Fig. 3).

These last equations, added to the system obtained for pavement layers equations, contribute to the general $5n(N+1)^2$ system equations of the following matrix form:

$$K_1.\mathbf{X} = K_2.\boldsymbol{\Sigma} + K_3 \qquad (34)$$

with K_1, K_2 and K_3 the matrices of dimensions $5n(N+1)^2 \times 5n(N+1)^2$, $5n(N+1)^2 \times 3(N+1)^2$ and $5n(N+1)^2 \times 1$, respectively.

Introducing cracks that are either longitudinal or transverse with respect to traffic load direction, or vertical over the thickness of one or several layers, requires considering that crack lips constitute two free edges, whose distance interval from one another is assumed nonzero, yet still narrow (on the order of one to several millimeters, depending on the type of pavement under examination). In the discretized diagram, the crack is numerically represented by a discontinuity between two lines of points marking the crack edges (see Fig. 4); this discontinuity is assumed to lie within the zone: $x \in [x_c,x_{c+1}]$ and $y \in [y_u,y_v]$, $1 \le u < v \le N+1$ $\forall$ $c \in [1,N]$. Indices u and v represent the crack beginning and end points in the plane for the specific layer numbers. For these crack lip point lines,

Bulletin des laboratoires des Ponts et Chaussées - 258-259
October-November-December 2005 - Ref. 4537 - pp. 105-120

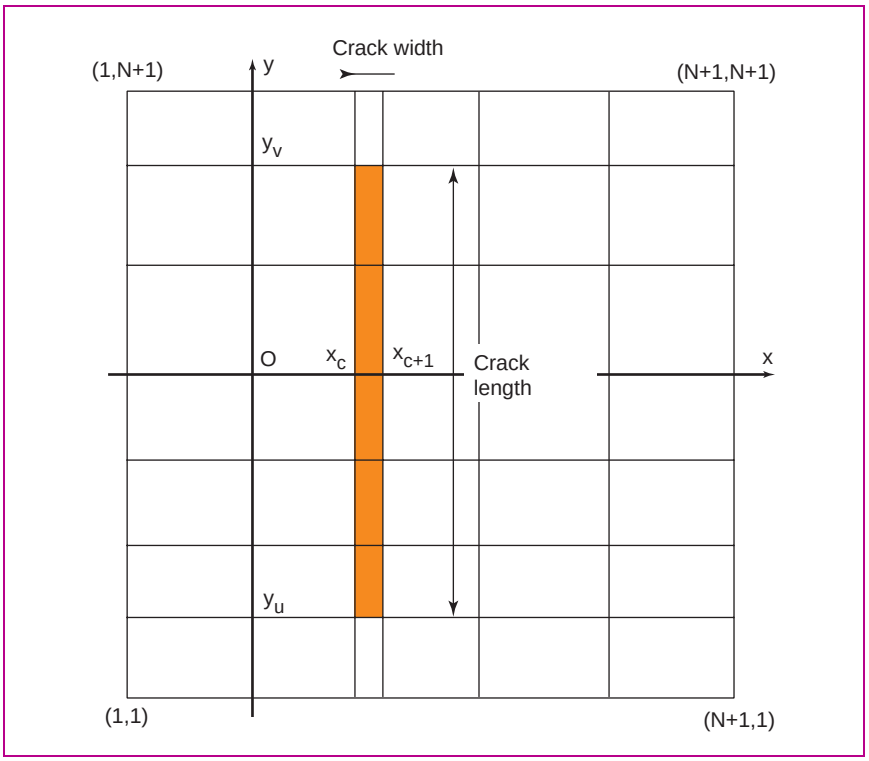

Figure 4
Crack introduction diagram in the M4-5nB computation plane

crack introduction into the previous system of equations (34) consists of deleting the corresponding equations and replacing them by boundary condition point lines of the free edge type given in previously-discretized systems (24) and (25).

Numerical resolution assessment of the M4-5nB model

From equations (33) and (34), the M4-5nB model can be summarized into a linear system with $(5n+3)(N+1)^2$ unsolved equations of the following form:

$$\begin{cases} \mathbf{X} = [K_1 - K_2 K_5^{-1} K_4]^{-1} . K_3 \\ \mathbf{\Sigma} = K_5^{-1} K_4 . \mathbf{X} \end{cases} \quad (35)$$

where: $\mathbf{X}$ and $\mathbf{\Sigma}$ are respectively the vector of kinematic unknowns with dimension $5n(N+1)^2$ and the vector of static unknowns with dimension $3(N+1)^2$ expressed above; K_1, K_2, K_4 and K_5 are respectively the material matrices of dimensions $5n(N+1)^2 \times 5n(N+1)^2$, $5n(N+1)^2 \times 3(N+1)^2$, $3(N+1)^2 \times 5n(N+1)^2$ and $3(N+1)^2 \times 3(N+1)^2$; and K_3 is the loading vector with dimension $5n(N+1)^2$.

For purposes of model validation, the ensuing resolution step was programmed by Tran [2004] using Matlab software.

VALIDATION WORK

As regards multilayered structures, many authors over the past 30+ years (particularly in the field of composite materials) have demonstrated that the presence of free edges or cracks, in conjunction with material behavior heterogeneity on both sides of interlayer interfaces, leads to significant out-of-plane stress concentrations at the interfaces (see for example [Pagano, 1978] or [Leguillon and Sanchez-Palencia, 1985]). This phenomenon requires further study before structural failure can be effectively predicted. Thus, in the aim of lightening the presentation of computation validation results, it was decided to proceed by illustrating just those results determined on out-of-plane stress fields at the interfaces. Chabot [1997], Carreira *et al.* [2002] and Tran [2004] have displayed validations of the other M4-5n and M4-5nB fields in comparison with 3D finite element-based computations.

In the following section on examples considered, the loading is expressed in the form of a uniform pressure on a square surface with side length 2a or on a rectangular surface of length 2a (along the traffic direction) and width 2b. The semi-infinite elastic soil mass has mechanical characteristics of the French class 2 supporting platform, with a Young's modulus E_s = 50 MPa and Poisson's ratio υ_s = 0.35 [LCPC-SETRA, 1994]. Depending on the specific case, computations are compared with either the 2D axisymmetric computation results from the "Alizé" software or the 3D finite element results from the CESAR-LCPC code.

Uncracked 3D case: An elastic layer lying on a soil mass

In this first case, the selected load corresponds to the French reference load of a truck wheel from a 65-kN dual-wheel half-axle [LCPC-SETRA, 1994]; it has been equivalently split for the axisymmetric computations performed using Alizé and those performed with M4-5nB on a square surface of side length a = 0.11079 m and pressure q = 0.662 MPa. An elastic layer with e_c = 0.08 m, E_c = 5,400 MPa and υ_c = 0.35 lying on the category 2 supporting platform has also been considered herein.

The 3D finite element mesh, composed of 20-node volume elements, contains 16 × 16 in-plane mesh links and 18 links along the vertical. The transverse dimensions are equal to 2.4 m, i.e. 10 times the load radius on each side. The soil extends 6 meters deep.

For the M4-5nB mesh, just a 10 × 10 link pattern proves sufficient in the plane.

Figure 5 shows, in the y = 0 plane, pavement-soil interface stresses for M4-5nB compared with those from both the 3D finite element computations and Alizé (with an equivalent circular load surface in this latter case).

The results obtained display strong agreement for the Alizé software as well as the simplified M4-5nB modeling, i.e. about 100 times faster than using 3D finite elements. It should nonetheless be noted that shear intensity at the load edge has been overvalued in Burmister's axisymmetric case, in comparison with the finite element solution and with M4-5nB. This result is most likely due to the load configuration, which has not been distributed in the various models over the same surface (square for computations performed with finite elements and M4-5nB, circular for Alizé). A more

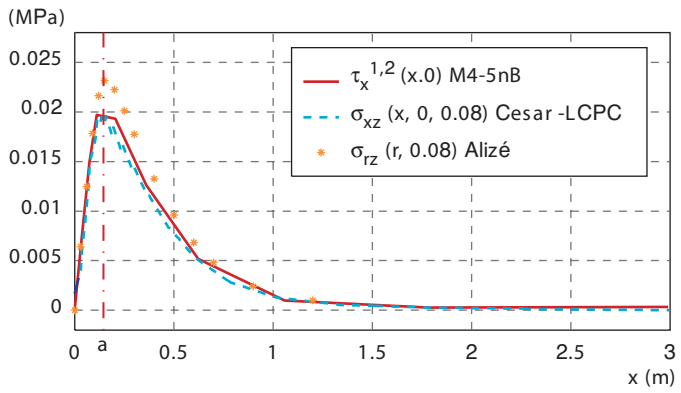

a. Shear

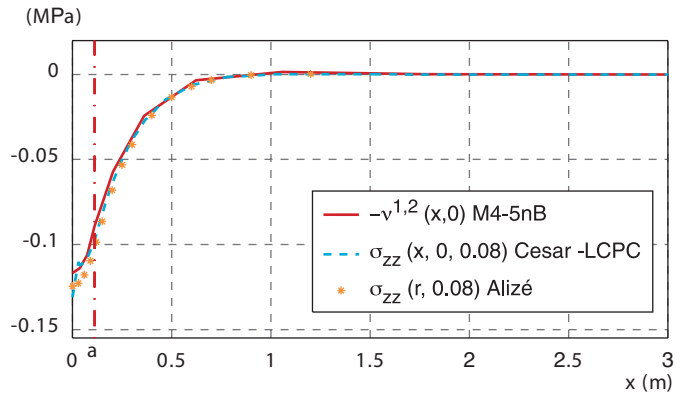

b. Normal

Figure 5

Uncracked 3D case: Comparison between M4-5nB model pavement-soil interface stresses, those from 3D finite element computations and those output by the Alizé software with an equivalent circular load

in-depth and realistic analysis of loading distributions and their corresponding surfaces during tire-pavement contact is a definite prerequisite to extending these hypotheses; other LCPC research projects currently focus on this aspect.

Case of the 3D bilayer of vertically-cracked pavement at the bottom

While remaining within the domain of linear elasticity, different loading cases may be superimposed. To identify the stress state underneath a crack during displacement of the rolling load, it would suffice to examine the case where the load is positioned adjacent to the crack, as described in Figure 6, i.e. where the crack does not reach the ground surface.

Figure 7 displays validations of a semi-rigid pavement structure cracked "from the bottom-up". The load is presumed to be rectangular (a = 0.15 m and b = 0.11 m) and of a pressure q = 0.662 MPa. The pavement is composed of 2 elastic layers (e_1 = 0.1 m, E_1 = 9,300 MPa, υ_1 = 0.35; e_2 = 0.3 m, E_2 = 23,000 MPa, υ_2 = 0.35) lying on top of the soil mass.

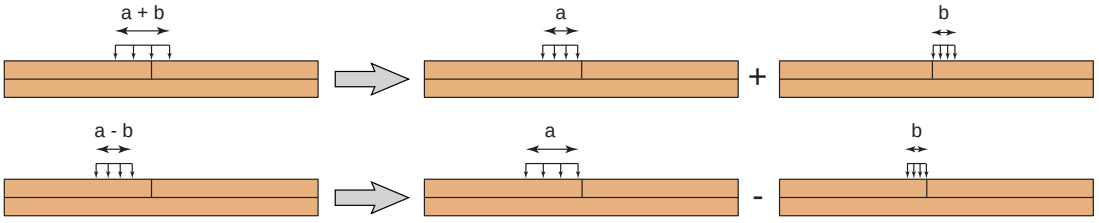

Figure 6
Loading decomposition diagram

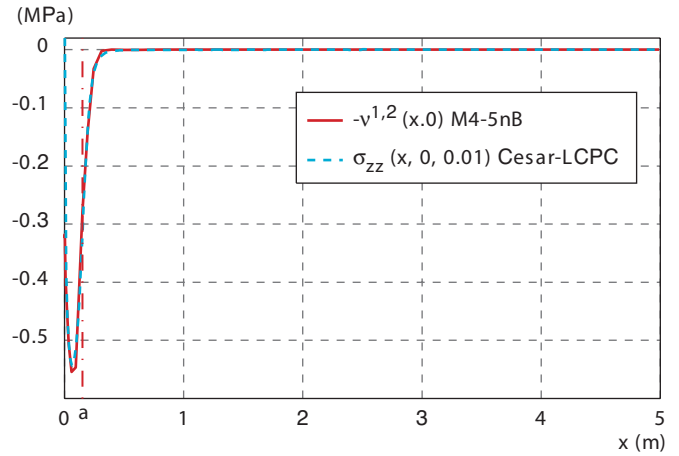

a. Interface 1,2

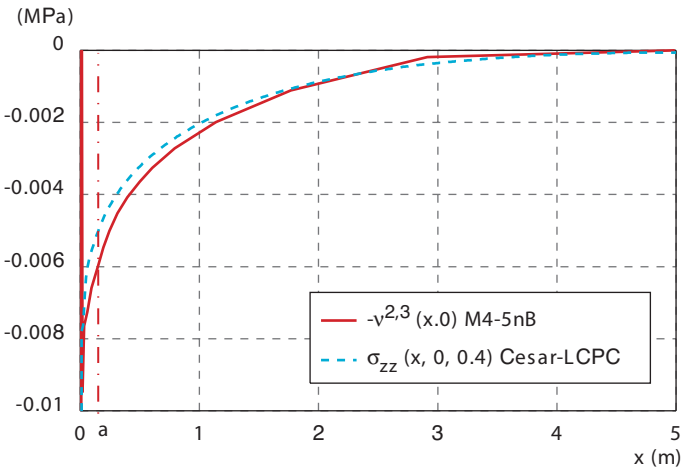

b. Interface 2,3

Figure 7
Comparison, for y = 0 at the interlayer interfaces, of normal stresses from the M4-5nB model and those yielded by 3D finite element computations (second cracked layer case)

The 3D finite element mesh comprises a total of 1,965 20-node volume elements and 7,080 15-node elements. Outside the loading zone, elements contain 15 nodes, with maximum intervals of 1 to 0.03 m. Under both load and crack, the mesh features 4×7 cubic links in the plane. 20 links are laid out along the layer stacking height. Soil depth equals 10 m. A 5-m transverse dimension ensures the sufficiency condition is being met.

The M4-5nB plane mesh contains 24×32 links. Blocked edge-type boundary conditions have been chosen for this procedure.

The computation of cracked pavement, assumed two-dimensional for this model set-up, reveals a very close approximation of stress fields at the various interfaces (see Fig. 7). The solution, programmed using Matlab, is obtained by M4-5nB roughly 10 times faster than that derived from a finely-meshed 3D finite element computation near the crack. Applying this vertical cracking configuration at the base of the dual pavement layer has enabled analyzing stresses as part of a research study on the reinforcement of semi-rigid pavements [Florence *et al.*, 2004].

APPLICATION TO THE 3D STRESS ANALYSIS OF A COMPOSITE PAVEMENT VERTICALLY CRACKED AT THE TOP

As a joint effort with the cement industry and in the aim of improving the design of composite structures (cement concrete on a gravel-bitumen mix) capable of being substituted for conventional pavements, the durability of the "White/Black" bonding has been studied [de Larrard *et al.*, 2001; Pouteau *et al.*, 2004]. Tests in the laboratory, on an actual pavement section and using the FABAC project equipment, were implemented and then analyzed [Pouteau, 2004]. To determine the constitutive law in fatigue of the bonding, application of the simplified M4-5n model makes it possible to optimally design, from a failure perspective, the dual-material laboratory specimens for inciting delamination [Pouteau *et al.*, 2002].

Among the various tests devised along these lines, the linear accelerated fatigue (FABAC) test was conducted on an actual platform through the end of 2003 at the LCPC's Nantes facility. Details on the instrumentation layout and COLIBRI non-destructive diagnostic results from the various test tracks have been provided in [Pouteau *et al.*, 2005] [Pouteau *et al.*, 2006]. Moreover, analysis of stress fields by means of M4-Boussinesq computations for the first cracked layer can contribute to results interpretation.

The following section will present, for illustration purposes, an initial elastic approximation of these results via the M4-5nB model programmed in its "*Research*" version and run using the Matlab tool [Tran, 2004; Guillo, 2004], in the case of blocked edges [Chabot *et al.*, 2004]. For this framework in the $y = 0$ plane, at the "white/black" interface of the composite pavement (made of thin bonded cement concrete), when the load is positioned at the crack edge, both normal and shear stresses of the M4-5n-B computation may be illustrated (see Fig. 8). The load is considered rectangular ($a = 0.14$ m and $b = 0.09$ m) with a pressure $q = 0.645$ MPa, while the pavement is considered to be composed of two elastic layers 1.95 m wide (category 5 cement concrete: $e_1 = 0.08$ m, $E_1 = 36{,}500$ MPa, $\upsilon_1 = 0.25$; asphalt overlay of the GB3 type: $e_2 = 0.095$ m, $E_2 = 8{,}485$ MPa, $\upsilon_2 = 0.35$) on top of the soil mass (infinite within the plane) of the PF3 type: $E_s = 120$ MPa, $\upsilon_s = 0.35$. The crack through the total thickness of the cement concrete layer displays an opening of 0.005 m, which corresponds with sawing the joint in the transverse direction.

The M4-5nB plane mesh contains 30×20 links.

In this loading position at the crack edge (with the crack centered at zero on Figures 8a and b), it can be observed that the pavement is loaded in mixed mode. This result justifies the laboratory failure test on a dual-material specimen in alternated bending developed as part of Pouteau's research [2004]. A sizable interface shear detected on the load edges gets accentuated by the presence of a crack. Moreover, the normal interface stress is highly negative underneath the load; it remains significant in tension on the unloaded side. It is clear that these results need to be examined in greater detail under actual experimental conditions (free edges along the *y*-axis; inclusion of thermal gradient effects in the thin bonded cement concrete layer and of the actual distribution of tire/pavement contact; comparison with instrumentation-based measurements; analysis of viscoelastic effects from gravel-bitumen and from debonding at the interlayer interface, etc.). These avenues of investigation have been addressed in recent LCPC research projects.

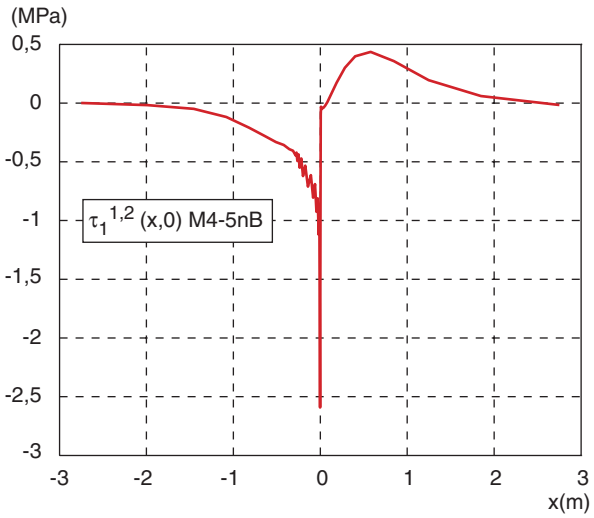

a. Shear interface stress

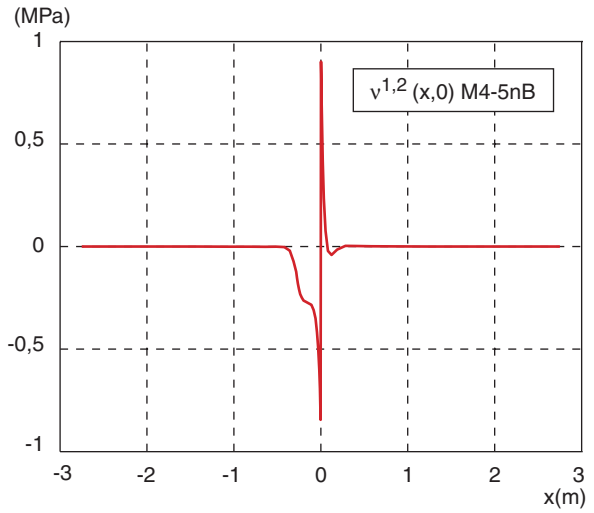

b. Normal interface stress

Figure 8
M4-5nB interface stresses for y = 0 along the "white/black" interface (first cracked layer case)

CONCLUSION

A simplified cracked pavement model, denoted M4-5nB (for multiparticle model of multilayered materials with 5*n* equilibrium equations - with *n* being the total number of pavement layers - lying on a Boussinesq soil mass) has been proposed as the computational core of a software intended for worn pavement diagnostic and maintenance. The problem of an actual 3D pavement structure can be reduced to determining five plane kinematic fields per pavement layer and three static fields at the pavement-soil interface, thereby transforming the real 3D object into a 2D geometric object. Put otherwise, expression of the initial 3D problem gets simplified to solving a 2D problem laid out in the plane composed of 5n + 3 equations with 5n + 3 unknown plane fields. The resolution process for this set of equations entails discretizing the 2D surface stemming from the simplified model into several elementary surfaces. Integrating Boussinesq's three analytical equations requires assuming that each integral can be evaluated by the sum of integrals over the elementary surfaces; in presuming that interface forces remain constant over such surfaces, these equations are then integrated analytically by means of simple variable changes. Following integration of the various boundary conditions, the remaining 2nd-order differential equations are solved by use of a finite differences diagram. The complete algorithm has been programmed in its "*Research*" version under Matlab [Tran, 2004]. This model yields very good approximations of the stress fields to be studied in the aim of predicting failure of the cracked pavement structures, while holding computation times considerably below those associated with finite element computations.

To produce a software for distribution throughout France's Ponts et Chaussées technical network and to further compress computation times for crack propagation analysis applications, a programming set-up running in a standard environment is currently under study. To accelerate the solution process even further within the scope of multicycle computations, a method for extrapolating 2D results in order to estimate 3D results has been proposed; based on a set of adimensional variables from the real 3D problem for a given range of materials and layer thicknesses, this method consists of listing the 3D results in tables or grids of desired field values [Tran *et al.*, 2004]. In the case of the cracked 3D bilayer, a 100-fold gain (instead of the current 10-fold gain) in comparison with a detailed 3D finite element analysis is being sought.

Finally, the examples cited herein have assumed that pavement layers were bonded both to one another and with the ground. It was also considered that the pavement was not being submitted to either temperature gradients or thermal shrinkage phenomena. The model described and forwarded in Tran's thesis [2004] has enabled expressing debonding. Thermal loadings and thermal shrinkage phenomena have been integrated and validated with respect to finite element computations. Research is now underway to apply these results and extend the initiation and propagation criteria for pavement cracks.

References

BATZ-VILLARD, *Influence des défauts de liaison sur le dimensionnement et le comportement des chaussées,* Thèse de doctorat spécialité génie civil, Université de Nantes, **1991**, 201 pages.

BODIN D., PIJAUDIER-CABOT G., DE LA ROCHE C., PIAU J.-M., CHABOT A., A continuum Damage Approach to Asphalt Concrete Modelling, *Journal of Engineering Mechanics (ASCE),* **130** (6), **2004**, pp. 700-708.

BURMISTER D.M., The theory of the stress and displacements in layered systems and applications of design of airport runway, *Proceeding of the Highway Research Board,* **23**, **1943**, pp. 126-148.

CARON J. F., DIAZ DIAZ A., CARREIRA R. P., CHABOT A., EHRLACHER A., Multiparticular modeling for the prediction of delamination in multiplayer, *Composites Sciences and Technology,* **66** (6), **2006**, pp. 755-765.

CARREIRA R. P., CARON J.-F., DIAZ DIAZ A., Model of multilayered materials for interface stresses estimation and validation by finite element calculations, *Mechanics of Material,* **34**, **2002**, pp. 217-230.

CHABOT A., *Analyse des efforts à l'interface entre les couches des matériaux composites à l'aide de Modélisations Multiparticulaires des Matériaux Multicouches (M4),* Thèse de doctorat spécialité structures et matériaux, École Nationale des Ponts et Chaussées, **1997,** 177 pages.

CHABOT A., EHRLACHER A., Modèles Multiparticulaires des Matériaux Multicouches M4_5n et M4_(2n+1)M pour l'étude des effets de bord, *Comptes-rendus aux 11e Journées Nationales sur les Composites (JNC11),* **3,** Arcachon, novembre **1998**, pp. 1389-1397.

CHABOT A., CANTOURNET S., EHRLACHER A., Analyse de taux de restitution d'énergie par un modèle simplifié pour un quadricouche en traction fissuré à l'interface entre deux couches, *Comptes-rendus aux 12e Journées Nationales sur les Composites (JNC12),* **2**, ENS de Cachan, novembre **2000**, pp. 775-784.

CHABOT A., TRAN Q.D., POUTEAU B., Simplified modelling of a cracked composite pavement, *First International Elsevier Conference on Failure Analysis*, Lisbonne, juillet **2004**.

De LARRARD F., POUTEAU B., CHABOT A., CLÉMENT J.-L., BALAY J.-M., Chaussées composites et nouvelles applications du ciment dans la route, *TPTech*, Paris, mars **2001**.

De LURDES ANTUNES M., Conclusions from COST 333 and Amadeus European projects : improvements to analytical pavement design models, *BCRA'02 workshop on modelling of flexible pavements,* Lisbonne, juin **2002**.

DUHAMEL D., NGUYEN V.H., CHABOT A., TAMAGNY P., Modelling of multilayer viscoelastic road structures under moving loads, *9th Int. Conf. on Civil and Structural Engineering Computing*, Amsterdam, septembre **2003**.

DUHAMEL D., CHABOT A., TAMAGNY P., HARFOUCHE L., ViscoRoute : Modélisation des chaussées bitumineuses, *Bulletin des laboratoires des Ponts et Chaussées*, **258-259**, octobre-novembre-décembre **2005**.

FLORENCE C., FORET G., TAMAGNY P., SENER J.-Y., EHRLACHER A., Experimental evaluation of reflextive cracking resistance in grid reinforced asphalt overlay, *Proceedings of the 5th Int. RILEM conf. Cracking in Pavements,* Limoges, mai **2004**.

GUILLO C. 2004, Validations par éléments finis d'un modèle simplifié pour l'étude de décollement à l'interface d'un multicouche de chaussée, Stage de DESS, Université de Nantes, **2004**, 52 pages.

JOHNSON K. L., *Contact Mechanics,* Cambridge University Press, **1992**.

LCPC-SETRA, *Conception et dimensionnement des structures de chaussée,* Guide Technique LCPC-SETRA, **1994.**

LEGUILLON D., SANCHEZ-PALENCIA E., Méthodes numériques appliquées à la mécanique, Une méthode numérique pour l'étude des singularités de bord dans les composites, *CR Acad. Sc.,* **301** (Série II, N° 18), **1985**.

NEWMARK N.M., A method of computation for structural dynamics, *ASCE J. of the Engineering Mechanics Division*, **85**, **1959**, pp. 67-94.

PAGANO N. J., Stress fields in Composite Laminates, *Int. J. Solids Structures*, **14**, **1978**, pp. 385-400.

POUTEAU B., CHABOT A., De LARRARD F., 2002, Étude en laboratoire du collage béton/ matériaux bitumineux, *Matériaux 2002*, Tours, **2002**.

POUTEAU B., *Durabilité mécanique du collage blanc sur noir dans les chaussée,* Thèse de doctorat spécialité génie civil, École Centrale de Nantes, **2004,** 213 pages.

POUTEAU B., BALAY J.-M., CHABOT A., De LARRARD F., Fatigue test and mechanical study of adhesion between concrete and asphalt, *9th Int. Symp. on Concrete Roads,* Istanbul, **2004.**

POUTEAU B., CHABOT A., BALAY J.-M., De LARRARD F., Essai accéléré de durabilité du collage blanc sur noir dans une chaussée composite, *17e Congrès Français de Mécanique*, Troyes, **2005**.

POUTEAU B., CHABOT A., De LARRARD F., BALAY J.-M., Étude de la dégradation du collage entre béton et enrobé sur une chaussée expérimentale à l'aide des simulateurs de trafic lourd FABAC, *Revue générale des routes et aérodromes (RGRA)*, **847**, **2006**, pp. 85-90.

REISSNER E., On a Variational Theorem in Elasticity, *J. Math. Phys.*, **29**, **1950**, pp. 90-95.

ROMANOSCHI S. A., LI Y., Experimental characterization and modeling of fatigue and crack propagation in asphalt concrete layers, *BCRA'02 workshop on modelling of flexible pavements,* Lisbonne, juin **2002**.

TRAN Q.D., *Utilisation des modèles multiparticulaires pour l'analyse des champs de contraintes dans une chaussée élastique,* Rapport de DEA, Université Paris VI, **2001**, 30 pages.

TRAN Q. D., CHABOT A., EHRLACHER A., TAMAGNY P., A simplified modelling for cracking in pavements, *Proceedings of the 5th Int. RILEM conf. Cracking in Pavements,* Limoges, mai **2004**.

TRAN Q.D., *Modèle simplifié pour les chaussées fissurées multicouches,* Thèse de doctorat spécialité structures et matériaux, École Nationale des Ponts et Chaussées, **2004,** 154 pages.

VANELSTRATE A., LEONARD D., VEYS J., Structural design of roads with steel treinforcing nettings, *Proceedings of the 4th Int. RILEM conf. Cracking in Pavements*, Ottawa, mars **2000**, pp. 57-67.